1

Fundamentals of Ray Tracing

A ray is defined as the collection of straight-line path segments followed by an energy bundle from its point of emission to its point of absorption. The definition includes the possibility of intermediate reflection, scattering, refraction, and even diffraction events. Ray tracing involves the application of basic mathematics to the process of identifying the intersection of ray segments with surfaces. Most engineering and science students acquire the required mathematical tools long before they enter university. The current chapter provides a review of the mathematical principles governing ray tracing and the related issues of meshing and indexing.

1.1 Rays and Ray Segments

A **ray** is defined here as the continuous sequence of straight-line paths connecting a point on one surface, from which an energy bundle is emitted, to a point on a second surface – or perhaps even on the same surface – where it is ultimately absorbed. One or several reflections from intervening surfaces may occur between emission and absorption of the energy bundle. The path followed by the energy bundle between

The Monte Carlo Ray-Trace Method in Radiation Heat Transfer and Applied Optics, First Edition. J. Robert Mahan.

This Work is a co-publication between John Wiley & Sons Ltd and ASME Press.
Companion website: www.wiley.com/go/mahan/monte-carlo

reflections is referred to as a **ray segment**. Two situations are normally considered: either (i) the power of the emitted energy bundle does not change as it is reflected from one surface to the next until it reaches the surface where all its power is ultimately absorbed; or (ii) a fraction of the emitted power is left behind with each reflection until the remaining power is deemed to have dropped below a threshold value, at which point the ray trace is terminated. Both approaches have their adherents and are in common use, and both are developed in detail in this book.

1.2 The Enclosure

The **enclosure** is an essential concept in all approaches to radiation heat transfer analysis. We define the enclosure as an ensemble of surfaces, both real and imaginary, arranged in such a manner that a ray emitted into the interior of the enclosure cannot escape. Energy is conserved within the enclosure under this definition. If a ray does leave the enclosure through an opening, represented by an imaginary surface, the energy it carries is deducted from the overall energy balance.

1.3 Mathematical Preliminaries

Consider two points, P_0 and P_1, in three-dimensional space, as illustrated in Figure 1.1. Let the Cartesian coordinates of points P_0 and P_1 be (x_0, y_0, z_0) and (x_1, y_1, z_1), respectively. Then the vector directed from P_0 to P_1 is

$$\boldsymbol{V} = (x_1 - x_0)\,\boldsymbol{i} + (y_1 - y_0)\,\boldsymbol{j} + (z_1 - z_0)\,\boldsymbol{k}, \tag{1.1}$$

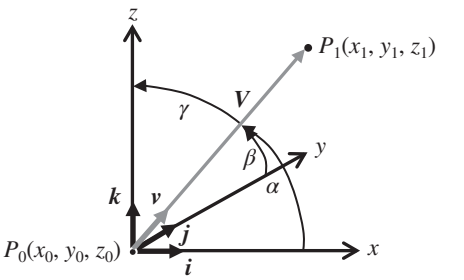

Figure 1.1 Relationships among the quantities introduced in Section 1.3.

and its magnitude is

$$t \equiv \sqrt{|\boldsymbol{V} \cdot \boldsymbol{V}|} = \sqrt{(x_1 - x_0)^2 + (y_1 - y_0)^2 + (z_1 - z_0)^2}. \tag{1.2}$$

In Eq. (1.1) $\boldsymbol{i}, \boldsymbol{j}$, and $\boldsymbol{k}$ are the unit vectors directed along the x-, y-, and z-axes, respectively. Note that the distance t from P_0 to P_1 must always be real and positive.

The unit vector in the direction of $\boldsymbol{V}$ is

$$\boldsymbol{v} \equiv \boldsymbol{V}/t = L\boldsymbol{i} + M\boldsymbol{j} + N\boldsymbol{k}, \tag{1.3}$$

where L, M, and N are the **direction cosines** illustrated in Figure 1.1. The direction cosines are defined

$$L \equiv \boldsymbol{v} \cdot \boldsymbol{i} = \cos\alpha, M \equiv \boldsymbol{v} \cdot \boldsymbol{j} = \cos\beta, \text{and } N \equiv \boldsymbol{v} \cdot \boldsymbol{k} = \cos\gamma, \tag{1.4}$$

where α, β, and γ are the angles between the unit vector $\boldsymbol{v}$ and the x-, y-, and z-axes, respectively. Equations (1.1) and (1.3) can be combined to define the equations for the line segment connecting point P_0 to point P_1

$$(x_1 - x_0)/L = (y_1 - y_0)/M = (z_1 - z_0)/N = t. \tag{1.5}$$

The three equations embodied in Eq. (1.5) are arguably the most important relationships in geometrical optics, because they form the basis for navigation of rays within an enclosure.

The general equation for a **surface** in Cartesian coordinates is

$$S(x, y, z) = 0. \tag{1.6}$$

The simplest, and perhaps most common, surface used in fabricating an enclosure is the plane, illustrated in Figure 1.2. In order to derive the equation for a plane, we must know the unit normal vector $\boldsymbol{n}$ at a point

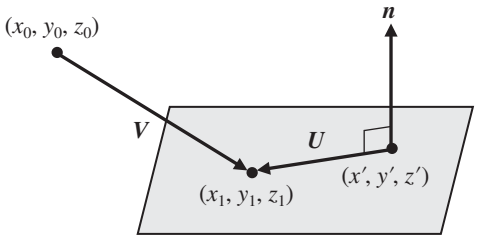

Figure 1.2 Definition of a plane surface.

(x', y', z') in the plane and the coordinates of a second point (x_1, y_1, z_1) in the plane. Then, because $\boldsymbol{n}$ and $\boldsymbol{U}$ are in quadrature, it must be true that

$$\begin{aligned} S(x_1, y_1, z_1) &= \boldsymbol{n} \cdot \boldsymbol{U} \\ &= \boldsymbol{n} \cdot [(x_1 - x')\,\boldsymbol{i} + (y_1 - y')\,\boldsymbol{j} + (z_1 - z')\,\boldsymbol{k}] \\ &= 0, \end{aligned} \tag{1.7}$$

or

$$S(x_1, y_1, z_1) = n_x\,(x_1 - x') + n_y\,(y_1 - y') + n_z\,(z_1 - z') = 0. \tag{1.8}$$

To find the intersection of the ray segment $\boldsymbol{V} = (x_1 - x_0)\,\boldsymbol{i} + (y_1 - y_0)\,\boldsymbol{j} + (z_1 - z_0)\,\boldsymbol{k}$ with the plane, we introduce Eq. (1.5) into Eq. (1.8), obtaining

$$n_x\,(x_0 + Lt - x') + n_y\,(y_0 + Mt - y') + n_z\,(z_0 + Nt - z') = 0. \tag{1.9}$$

Finally, solving Eq. (1.9) for t we obtain

$$t = \frac{n_x(x' - x_0) + n_y(y' - y_0) + n_z(z' - z_0)}{n_x L + n_y M + n_z N}, \tag{1.10}$$

or

$$t = \frac{\boldsymbol{n} \cdot (\boldsymbol{V} - \boldsymbol{U})}{\boldsymbol{n} \cdot \boldsymbol{v}}. \tag{1.11}$$

Note that if $\boldsymbol{n}$ and $\mathbf{v}$ are in quadrature, $\boldsymbol{n} \cdot \boldsymbol{v} = 0$, in which case t is undefined. The interpretation is that the ray passes parallel to the plane and so can never intersect it. We must anticipate this eventuality when programming. This is perhaps an appropriate juncture to emphasize the natural compatibility of Cartesian coordinates with the vector nature of ray tracing.

A more instructive example is the intersection of a ray segment with a sphere of radius R whose center is located at (x_C, y_C, z_C); that is,

$$S(x_1, y_1, z_1) = (x_1 - x_C)^2 + (y_1 - y_C)^2 + (z_1 - z_C)^2 - R^2 = 0. \tag{1.12}$$

Suppose a ray is emitted from point (x_0, y_0, z_0) in the direction (L, M, N) and we want to find its point of intersection (x_1, y_1, z_1) with this sphere. As in the previous example, this may be accomplished by finding the point (x_1, y_1, z_1) that simultaneously satisfies the three equations for the straight line connecting the two points, Eq. (1.5), and the equation for the sphere, Eq. (1.12); that is,

$$(x_0 + Lt - x_C)^2 + (y_0 + Mt - y_C)^2 + (z_0 + Nt - z_C)^2 - R^2 = 0. \tag{1.13}$$

Happily, the solution of Eq. (1.13) for the distance t is just about the most challenging mathematical operation we encounter in ray tracing.

It is convenient to use the symbolic solver feature of Matlab to solve quadratic equations (see Problems 1.2–1.7). However, solution of Eq. (1.13) is relatively straightforward and provides an opportunity to point out certain useful properties of the quadratic coefficients. Upon carrying out the indicated operations and rearranging the result, we have

$$(L^2 + M^2 + N^2)\, t^2 + 2[L(x_0 - x_C) + M(y_0 - y_C) + N(z_0 - z_C)]\, t + (x_0 - x_C)^2 + (y_0 - y_C)^2 + (z_0 - z_C)^2 - R^2 = 0, \tag{1.14}$$

or

$$A\, t^2 + B\, t + C = 0, \tag{1.15}$$

where

$$A = L^2 + M^2 + N^2, \tag{1.16}$$

$$B = 2[L(x_0 - x_C) + M(y_0 - y_C) + N(z_0 - z_C)], \tag{1.17}$$

and

$$C = (x_0 - x_C)^2 + (y_0 - y_C)^2 + (z_0 - z_C)^2 - R^2. \tag{1.18}$$

The coefficients A, B, and C are defined in terms of known quantities and, thus, are themselves known. Equation (1.14) can now be solved for t, yielding

$$t_1 = (-B + \sqrt{B^2 - 4AC})/2A \text{ and } t_2 = (-B - \sqrt{B^2 - 4AC})/2A. \tag{1.19}$$

We define a **quadratic surface** as any surface whose algebraic equation $S(x, y, z) = 0$ is second-order. It turns out that, in addition to plane surfaces, essentially all enclosures of practical engineering interest include such surfaces or surfaces that can be subdivided into such surfaces. Listed in Table 1.1 are some of the quadratic surfaces commonly encountered in radiation heat transfer and applied optics. Equation (1.19), with generally different expressions for the coefficients A, B, and C, yields the candidate values of the distance t for all quadratic surfaces.

Note that Eq. (1.19) has two roots, t_1 and t_2. The physical interpretation of two roots is that a given ray "intersects" the spherical surface at two points. However, the intersection may be **degenerate** (both roots corresponding to the same point) or **imaginary** (the ray does not physically intersect the sphere). Only in the case of plane surfaces are single,

Table 1.1 Quadratic surfaces commonly encountered in radiation heat transfer and applied optics modeling.

Name	$S(x, y, z) = 0$	Notes
Sphere	$(x-x_C)^2+(y-y_C)^2+(z-z_C)^2-R^2=0$	R = radius, center at (x_C, y_C, z_C)
Tri-axial ellipsoid	$\frac{(x-x_C)^2}{a^2}+\frac{(y-y_C)^2}{b^2}+\frac{(z-z_C)^2}{c^2}-1=0$	a, b, c = semi-axes, center at (x_C, y_C, z_C)
Spheroid	$\frac{(x-x_C)^2}{a^2}+\frac{(y-y_C)^2}{a^2}+\frac{(z-z_C)^2}{c^2}-1=0$	Prolate if $c > a$, oblate if $c < a$, center at (x_C, y_C, z_C)
Elliptic paraboloid	$\frac{(x-x_C)^2}{a^2}+\frac{(y-y_C)^2}{b^2}-z=0$	Upward-opening, origin at (x_C, y_C, z_C)
Hyperbolic paraboloid ("Potato chip")	$(x/a)^2-(y/b)^2-z=0$	Opens up along x-axis, down along y-axis
Two-sheet hyperboloid	$(x/a)^2+(y/a)^2-(z/c)^2+1=0$	Rotationally symmetric about z-axis
Right-circular cone	$(x-x_v)^2+(y-y_v)^2 - tan^2\alpha\,(z-z_v)^2=0$	Vertex at (x_v, y_v, z_v), α = cone half-angle
Right-circular cylinder	$x^2+y^2-R^2=0,\ 0\le z\le h$	Rotationally symmetric about z-axis, h = height

non-degenerate roots obtained. More than two roots arise in the case of higher-order surfaces but, as has already been pointed out, most enclosures of practical engineering interest are composed of either planes or quadratic surfaces.

The physical significance of quadratic roots is illustrated in Figure 1.3. If both roots are real ($B^2 > 4AC$) in Eq. (1.19), the ray emitted from P_0 intersects the surface at two points, P_1 and P_2, where one corresponds to the plus (+) sign in Eq. (1.19) and the other corresponds to the minus (−) sign. If $B^2 = 4AC$, the roots are degenerate and the single solution, $t = -B/2A$, is obtained. This signifies that the ray is tangent to the sphere at a single point P_3. Finally, if both roots are complex ($B^2 < 4AC$), the ray fails to intersect the surface.

At the most, only one real root is physically significant. How do we choose between the two available real roots? This is a trivial choice for someone provided with an image such as Figure 1.3; however, a computer requires an algorithm based on the values of the quadratic coefficients A, B, and C. In the special case of a sphere we recognize that $A = \sqrt{\boldsymbol{v} \cdot \boldsymbol{v}} = 1$, where the vector $\boldsymbol{v}$ is given by Eq. (1.3). While this simplifies the algebra somewhat, it does not otherwise contribute to the process of identifying the correct root. The coefficient B in the case of a sphere can be expressed

$$B/2 = \boldsymbol{v} \cdot \boldsymbol{V}_0, \tag{1.20}$$

where $\boldsymbol{V_0}$ is the vector directed from the center of the sphere (x_C, y_C, z_C) to the source point (x_0, y_0, z_0),

$$\boldsymbol{V}_0 = (x_0 - x_C)\,\boldsymbol{i} + (y_0 - y_C)\,\boldsymbol{j} + (z_0 - z_C)\,\boldsymbol{k}. \tag{1.21}$$

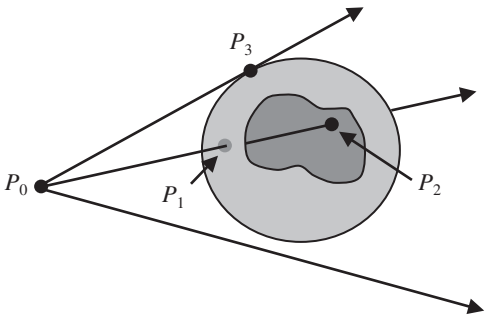

Figure 1.3 Possible disposition of three rays emitted from point P_0.

The value of the coefficient C determines whether the source point is interior to the sphere ($C<0$), exterior to the sphere ($C>0$), or lies in the surface of the sphere ($C=0$). It has already been pointed out that the value of the argument of the square root in Eq. (1.19), $B^2 - 4AC$, determines whether or not the ray intersects the sphere. In the case of real roots, including degenerate roots, the interplay between the B and C coefficients determines the sign choice, as demonstrated in the following example.

Figure 1.4 depicts candidate rays in the interior of the hollow sphere defined by Eq. (1.12). The location of the origin of coordinates (0, 0, 0) is immaterial in the following argument. The ray source point (x_0, y_0, z_0), the sphere center (x_C, y_C, z_C) and radius R, and the components of the unit vector $\boldsymbol{v} = (L, M, N)$ are all assumed known. Because the ray source point is interior to the sphere, we find that $C<0$. It follows that $B^2 - 4AC > 0$ regardless of the value of B. Therefore, there exist two real roots, corresponding to the two candidate intersections at (x_u, y_u, z_u) and (x_d, y_d, z_d).

The unit normal vector on the interior surface of the sphere is given by

$$\boldsymbol{n} = -\frac{\nabla S}{|\nabla S|} = -\left(\frac{x-x_c}{R}\right)\boldsymbol{i} - \left(\frac{y-y_c}{R}\right)\boldsymbol{j} - \left(\frac{z-z_c}{R}\right)\boldsymbol{k} = -\frac{1}{R}(\boldsymbol{V} + \boldsymbol{V}_0). \tag{1.22}$$

Then it can be demonstrated (see Problem 1.10) that

$$\boldsymbol{v}\cdot\boldsymbol{n} = -\frac{1}{R}\left(t + \frac{B}{2}\right). \tag{1.23}$$

In order for a ray emitted from point (x_0, y_0, z_0) in direction (L, M, N) to intercept the wall of the spherical shell at point (x, y, z), it must be true that $\boldsymbol{v}\cdot\boldsymbol{n} < 0$ (see Problem 1.11). We conclude that the correct sign in Eq. (1.19) is the one that leads to $t + b/2 > 0$; i.e., the "+" sign must be

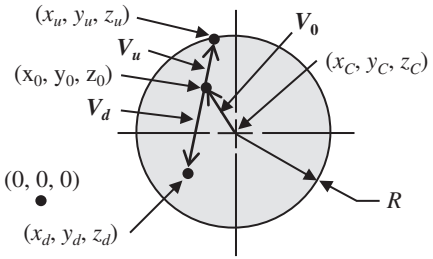

Figure 1.4 Candidate rays in the interior of the hollow sphere defined by Eq. (1.12).

selected in this case. It is emphasized that this is a general result for the case of a ray emitted from any position interior to a spherical enclosure.

The above example illustrates the important point that Eq. (1.5) describes an infinitely long line. In Figure 1.4 the upward-directed ray $\boldsymbol{V_u}$ and the downward-directed ray $\boldsymbol{V_d}$ both lie on the same line. Therefore, the simultaneous solution of the equations for this line with the equation for the sphere necessarily leads to two roots and, thus, to two intersections, only one of which is relevant. The true point of intersection is the **forward candidate**, i.e., the one lying in the direction of $\boldsymbol{v}$ with respect to the source point. The incorrect point, which lies in the opposite direction of $\boldsymbol{v}$, is referred to as a **back candidate**. Identification and elimination of back candidates is a constant concern in ray tracing.

Suppose the situation shown in Figure 1.4 is modified so that the source point (x_0, y_0, z_0) lies on the same line except that it now lies outside the sphere. In this case both points of intersection can be forward candidates or both can be back candidates, depending on the direction of the emitted ray. How do we sort out these possibilities?

In Figure 1.5a it is obvious to the human observer that both points of intersection are forward candidates, while in Figure 1.5b both are clearly back candidates. Furthermore, it seems equally obvious – once again to the human observer – that in the case of two forward candidates, the one nearer the source, and thus corresponding to the smaller value of t, is the correct choice. But, in fact, this would be true only if it is the outer surface of the sphere that is optically active. All surfaces, being the locus of all points where $S(x, y, z) = 0$, are vanishingly thin. Therefore, a given

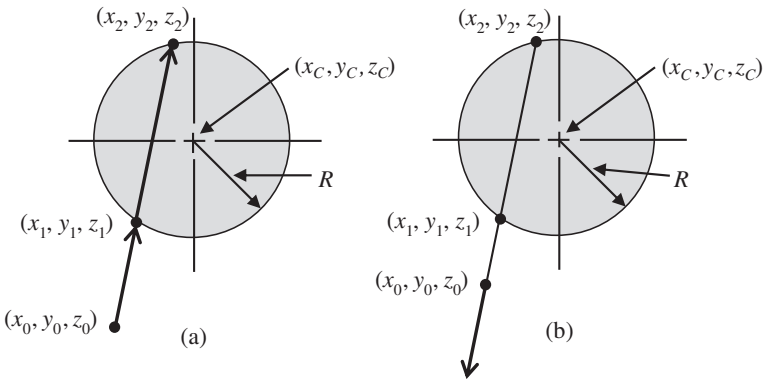

Figure 1.5 In (a) both points of intersection are forward candidates while in (b) both points of intersection are back candidates.

location (x_1, y_1, z_1) really represents *two* surfaces, or, more precisely, two sides of a single surface. Therefore, in Figure 1.5a the point (x_1, y_1, z_1) can represent either the inside surface or the outside surface of the sphere, depending on which surface is designated to be optically active. If the inside surface of the sphere in Figure 1.5a is deemed to be optically active, then the outside surface is mathematically transparent and point (x_2, y_2, z_2) rather than point (x_1, y_1, z_1) is the valid forward candidate.

The spherical sector in Figure 1.6 might represent a concave mirror used as an optical element, for example in a telescope. In this case its interior surface is considered to be a perfect mirror while its exterior surface, as well as the extended interior and exterior surfaces of the sphere from which the mirror is formed, indicated by the broken curve, simply do not exist. Given a ray originating at point (x_0, y_0, z_0), how do we determine (without looking at the figure) if it is reflected from the concave mirror?

Suppose simultaneous solution of Eqs. (1.5) and (1.12) yields the pair of real roots, t_1 and t_2, so that the corresponding coordinates for the candidate points are

$$x_1 = x_0 + Lt_1, y_1 = y_0 + Mt_1, \text{ and } z_1 = z_0 + Nt_1 \tag{1.24}$$

and

$$x_2 = x_0 + Lt_2, y_2 = y_0 + Mt_2, \text{ and } z_2 = z_0 + Nt_2. \tag{1.25}$$

How does the computer "know" which is the correct point? Bear in mind that these two intersections are actually two candidate points, one on the interior and one on the exterior of the spherical shell. In this case the point (x_1, y_1, z_1) (outside), which is the nearest to the source point, would be incorrect because it lies on the exterior surface while the concave mirror

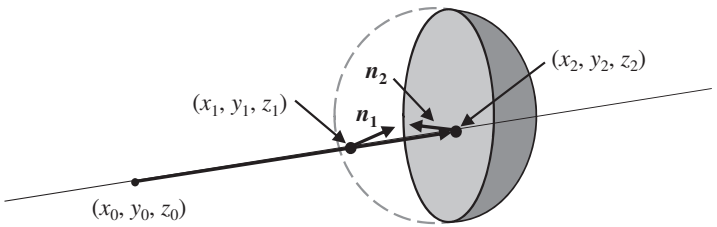

Figure 1.6 Instructing the computer to designate (x_2, y_2, z_2) rather than (x_1, y_1, z_1) as the point of intersection of the ray on the concave spherical sector.

is known to be a section of the interior surface. An essential feature of a successful Monte Carlo ray-trace (MCRT) program is that it must compute all intersections of all rays with all surfaces of the enclosure, and then sort through all of the resulting candidates to identify the right one. When the process arrives at the spherical-sector mirror shown in Figure 1.6, it initially treats it as a complete spherical shell having two exterior surfaces and two interior surfaces. Therefore, in the case of this particular surface, we must first instruct the computer to ignore the exterior surfaces and consider only the two interior surfaces.

How does the computer distinguish between exterior and interior surfaces? Firstly, it computes the local surface unit normal vector

$$\boldsymbol{n} = \pm \nabla S / |\nabla S|. \tag{1.26}$$

Following convention, the plus (+) sign is used in this calculation when the exterior surface is to be considered, while the minus (−) sign is used in the case of the interior surface. (The reader is cautioned that while the distinction between the exterior and the interior of a sphere is obvious, this is not always the case for many common quadratic surfaces.) In the example of Figure 1.6, the minus sign is used since the unit vector is pointed inward. Next the computer evaluates the sign of the dot product $\boldsymbol{v} \cdot \boldsymbol{n}$. We have already seen that the ray is directed away from any surface for which $\boldsymbol{v} \cdot \boldsymbol{n} > 0$ and is directed toward any surface for which $\boldsymbol{v} \cdot \boldsymbol{n} < 0$. Thus, in the current example, since $\boldsymbol{v} \cdot \boldsymbol{n_2} < 0$, it is clear to both the computer and its human operator that the ray is incident to the interior point (x_2, y_2, z_2) rather than to the exterior point (x_1, y_1, z_1).

The foregoing example makes it clear that the development of ray-tracing skills requires familiarity with geometry, trigonometry, and algebra as well as an appreciation for logic and possession of computer programming skills. Indeed, a modestly gifted high-school senior could master the basic skill set in a matter of a few days. It is only the sophistication of the rules governing the interaction of electromagnetic radiation with materials of practical engineering interest that elevates the material in this book to the advanced university level.

1.4 Ideal Models for Emission, Reflection, and Absorption of Rays

To this point we have treated the ray as a strictly mathematical concept without considering its physical nature. However, as we move on to the phenomena of emission, absorption, reflection, scattering, and refraction,

which occur when a ray intersects a surface, it will be convenient to introduce certain models borrowed from geometrical optics. In later chapters, we explore the principles of physical optics underlying these models. However, for the present it is convenient to exploit their relative simplicity as a tool for developing ray-tracing skills. This is not to say that the models introduced in this section are of pedagogical interest only; indeed, they have been the basis for traditional radiation heat transfer practice for the past century, during which time they have consistently yielded results whose accuracy is at least as good as that afforded by contemporary conduction and convection heat transfer epistemology.

We have been using the generally well understood term "surface" without formal definition. It is now appropriate to formally define a surface as the interface separating two regions of space having different optical properties. In fact, true surfaces do not exist, although approximations of surface behavior can be approached to an arbitrarily high degree of precision.

The optical behavior of a material substance is characterized by its **index of refraction** and its **extinction coefficient**. As a ray encounters the interface between two materials having different values of these optical properties, a portion of its power is redirected away from the interface. This portion of the incident power is said to be "reflected." Of the power that crosses into the second medium, a portion is said to be "absorbed" while the remainder is said to be either "scattered" or "refracted." The scattered and refracted power continues to propagate through the second medium while the absorbed power is locally converted into sensible heat. The two most prevalent models for describing reflection at a surface are the **specular reflection model** and the **diffuse reflection model**. These two models are important because they represent opposite extremes, both of which are often the desired behavior in engineering applications.

The specular reflection model, used to describe the ideal optical behavior of mirrors and certain other highly polished surfaces, is illustrated in Figure 1.7. In the figure, $\boldsymbol{v}$ and $\boldsymbol{n}$ are the unit vectors defined by Eqs. (1.3) and (1.26), respectively. The rule for specular reflection may be deduced by inspection of the figure; that is,

$$\boldsymbol{v_R} = \boldsymbol{v_I} - 2(\boldsymbol{v_I} \cdot \boldsymbol{n})\,\boldsymbol{n} = \boldsymbol{v_I} + 2\cos(\vartheta)\,\boldsymbol{n}, \tag{1.27}$$

where $\vartheta = \vartheta_I = \vartheta_R$. Note that the specular reflection model says nothing about the power of the reflected ray compared to that of the incident ray, although in the case of an ideal mirror they are assumed to be the same.

The diffuse reflection model, commonly used to describe the optical behavior of all non-specular surfaces, is illustrated in Figure 1.8. In the

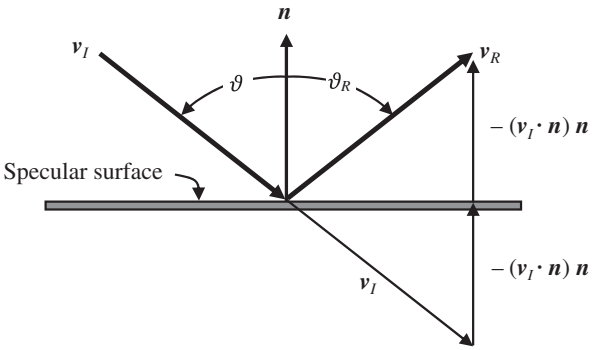

Figure 1.7 The specular reflection model.

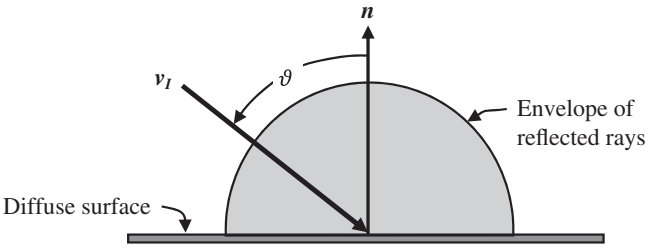

Figure 1.8 The diffuse reflection model.

MCRT interpretation of diffuse reflection, the reflected portion of the power contained in the incident ray $\boldsymbol{v_I}$ is redistributed into the hemispherical space above the point of incidence by a large but finite number of rays, where each ray carries the same power. In this case the directional distribution of the rays is governed by the values of a sequence of random numbers, as described later in this chapter. In principle, the number of directional components involved in such a reflection is infinite. However, in a practical ray trace, the number N of reflected components is necessarily finite, with each reflected component considered to carry a fraction $1/N$ of the total reflected power.

The diffuse reflection model may be extended to describe the directionality of emission and absorption. Theoretical considerations lead to the conclusion that if a surface is a diffuse reflector it must also be a diffuse absorber; that is the fraction of power absorbed from an incident ray is independent of the ray's direction. Furthermore, a diffuse absorber

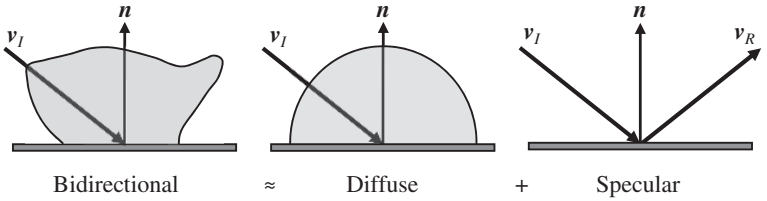

Figure 1.9 The diffuse–specular approximation of a bidirectional reflecting surface.

must also be a diffuse emitter, meaning that the directional distribution of emitted equal-power rays is governed by the same statistical rules that describe diffuse reflection. Finally, in the limiting case of a perfect absorber, all the incident radiation is absorbed. The opposite of a perfect absorber is the perfect reflector for which all the incident power is reflected.

In many cases of practical engineering interest, reflection from a surface can be modeled with acceptable accuracy as the sum of a diffuse component and a specular component, as illustrated in Figure 1.9. When using this model, emission and absorption could still be assumed diffuse, especially if the diffuse component of reflection is predominant. In any case, the analysis of an enclosure made up of directionally reflecting surfaces could always be improved by assuming diffuse–specular reflections, even if diffuse emission and absorption are retained.

More sophisticated models for emission, reflection, and absorption, which recognize that they are generally functions of both wavelength and direction, are considered in Chapter 4. The coefficients corresponding to these models provide sufficient information for rays to navigate from point to point along straight-line paths. The formal definition of the **bidirectional spectral reflectivity**, $\rho(\lambda, \vartheta_I, \varphi_I, \vartheta_R, \varphi_R)$, is given in Chapter 2. Its equivalent form in the MCRT environment addresses the question, "If a ray carrying one unit of power in wavelength interval $\Delta\lambda$ about wavelength λ is incident to a point on a surface from direction ϑ_I, φ_I, what fraction of the incident power is carried by a ray reflected from that point in direction ϑ_R, φ_R?" Its value for a specified combination of directions at a given wavelength is obtained by reference to a look-up table or to an empirical model. The bidirectional spectral reflectivity is mutually reciprocal in the sense that its incident and reflected directions can be interchanged without changing its value; i.e.,

$$\rho(\lambda, \vartheta_I, \varphi_I, \vartheta_R, \varphi_R) = \rho(\lambda, \vartheta_R, \varphi_R, \vartheta_I, \varphi_I). \tag{1.28}$$

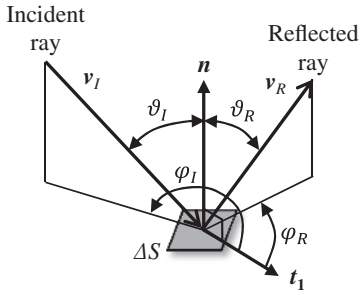

Figure 1.10 Nomenclature for incident and reflected rays.

We learn in Chapter 2 that all models for emission, reflection, and absorption follow from knowledge of the bidirectional spectral reflectivity.

Figure 1.10 illustrates the conventions for defining the incident and reflected directions. In the figure, the unit vector $\boldsymbol{t_1}$ is tangential to the surface element ΔS and is normal to the local unit normal vector $\boldsymbol{n}$.

It is often convenient to define the direction of the unit tangent vector such that

$$\boldsymbol{t}_1 = \boldsymbol{n} \times \boldsymbol{v_I} / |\boldsymbol{n} \times \boldsymbol{v_I}|, \tag{1.29}$$

since both $\boldsymbol{v_I}$ and $\boldsymbol{n}$ are known. However, the convention fails on those rare occasions when, to within the precision of the processor being used, $\boldsymbol{v_I} = -\boldsymbol{n}$. In this case, the denominator in Eq. (1.29) vanishes and the offending ray must either be discarded or slightly redirected. An alternative approach that avoids this weakness is presented in Chapter 3.

We define the **directional spectral emissivity** $\varepsilon(\lambda, \vartheta_E, \varphi_E)$ as the efficiency, compared to an ideal surface, with which a real surface emits thermal radiation, in wavelength interval $\Delta\lambda$ about wavelength λ, and in direction (ϑ_E, φ_E). The nature of the ideal surface referred to here is considered in Chapter 2. The **directional spectral absorptivity** $\alpha(\lambda, \vartheta_I, \varphi_I)$ is the fraction of incident thermal radiation in that wavelength interval, incident from direction (ϑ_I, φ_I), that is absorbed. It can be demonstrated that the directional spectral absorptivity is equal to the directional spectral emissivity at the same wavelength when $(\vartheta_I, \varphi_I) = (\vartheta_E, \varphi_E)$ [1].

Finally, the **directional-hemispherical spectral reflectivity** $\rho(\lambda, \vartheta_I, \varphi_I)$ is defined as the fraction of the power incident from direction (ϑ_I, φ_I) that is reflected into the hemispherical space above the point of incidence. The formal relationship between the directional-hemispherical

spectral reflectivity and the bidirectional spectral reflectivity is developed in Chapter 2. In the MCRT environment this relationship can be expressed

$$\rho(\lambda, \vartheta_I, \varphi_I) = 2\pi \sum \rho(\lambda, \vartheta_I, \varphi_I, \vartheta_R, \varphi_R)/N, \tag{1.30}$$

where N is the total number of reflected rays. Conservation of energy requires that, in the absence of forward scattering and refraction (i.e., for an **opaque** surface),

$$\alpha(\lambda, \vartheta_I, \varphi_I) = 1 - \rho(\lambda, \vartheta_I, \varphi_I). \tag{1.31}$$

Implementation of the definitions for these coefficients in terms of models of varying degrees of sophistication is the topic of Chapter 4. For now, the relatively simple specular and diffuse reflection models illustrated in Figures 1.7 and 1.8 are well suited to the pedagogical purposes of the current chapter. According to these models, $\rho(\lambda, \vartheta_I, \varphi_I) = \rho(\lambda$ *only)*, with $\vartheta_R = \vartheta_I$ and $\varphi_R = \varphi_I + \pi$ for specular surfaces and, for diffuse surfaces,

$$\vartheta_R = \sin^{-1}[\sqrt{R_\vartheta}] \text{ and } \varphi_R = 2\pi R_\varphi, \tag{1.32}$$

where in both cases the angles ϑ and φ are measured with respect to normal and tangent unit vectors, as indicated in Figure 1.10. In Eq. (1.32), R_ϑ and R_φ are random numbers uniformly distributed between zero and unity. Random number generation is treated more fully in the Appendix but the random-number generators available in most computing environments, for example *rand* in Matlab, are adequate for most applications.

Models for the remaining coefficients follow from their definitions. Thus, for opaque surfaces the directional spectral absorptivity $\alpha(\lambda, \vartheta_I, \varphi_I)$ becomes $\alpha(\lambda) = 1 - \rho(\lambda)$, and the directional spectral emissivity $\varepsilon(\lambda, \vartheta_E, \varphi_E)$ becomes $\varepsilon(\lambda) = \alpha(\lambda)$. In the case of a diffuse source the direction of emission is determined using Eq. (1.32) while, in the case of a directional source, rays are emitted with some specified directional distribution. For example, in the special case of a **collimated** source, *all* rays are emitted in a specified direction (ϑ_E, φ_E).

Bearing in mind that rays navigate using direction cosines, it would be useful if Eq. (1.32), with the "R" subscripts replaced with "E" subscripts, could be used to compute L, M, and N for the case of diffuse emission. For this purpose a second unit tangent vector $\boldsymbol{t_2}$ that is normal to both $\boldsymbol{n}$ and $\boldsymbol{t_1}$, is defined

$$\boldsymbol{t}_2 = \boldsymbol{n} \times \boldsymbol{t}_1. \tag{1.33}$$

It can then be demonstrated (see Problem 1.12) that

$$L = n_x \cos\vartheta_E + t_{1,x} \sin\vartheta_E \cos\varphi_E + t_{2,x} \sin\vartheta_E \sin\varphi_E,$$
$$M = n_y \cos\vartheta_E + t_{1,y} \sin\vartheta_E \cos\varphi_E + t_{2,y} \sin\vartheta_E \sin\varphi_E,$$
$$\text{and } N = n_z \cos\vartheta_E + t_{1,z} \sin\vartheta_E \cos\varphi_E + t_{2,z} \sin\vartheta_E \sin\varphi_E. \quad (1.34)$$

Finally, in some situations it is justified to assume that the surface model coefficients ε, α, and ρ are independent of wavelength. This so-called **graybody approximation** has dominated radiation heat transfer practice for the past century. Its enduring popularity stems from the fact that it significantly simplifies the analysis while remaining relevant in a wide range of practical applications. Therefore, in this introductory chapter to ray tracing we temporarily set aside the analytical complications imposed by wavelength-dependent surface models with the idea of adding them later as needed.

1.5 Scattering and Refraction

The power incident to a surface that is neither absorbed locally nor reflected is then either scattered in a process analogous to reflection, or it is refracted. In the MCRT description of radiation heat transfer, scattering is modeled by subdividing the incident ray into many equal-power rays, with each scattered ray continuing in a direction determined by an appropriate scattering model. The complex phenomenon of scattering is treated in detail in Chapter 5, which deals with radiation propagating through a **participating medium**. The simplest and most basic model for scattering, which is used in the early chapters of this book, is the assumption that scattering can be neglected, as is often the case in radiation heat transfer.

In the ray-trace description of geometrical optics, refraction refers to the abrupt change in direction of the transmitted ray as it passes through an interface. The Snell–Descartes law, illustrated in Figure 1.11, represents reality very well, especially for interfaces between air and common materials used in the fabrication of lenses, filters, retarder plates, and windows. According to the Snell–Descartes law

$$\sin(\vartheta_1)/\sin(\vartheta_2) = n_2/n_1, \quad (1.35)$$

where n_1 and n_2 are the refractive indices of the two materials whose interface provokes refraction. Problem 1.14 is an important application of this principle in applied optics.

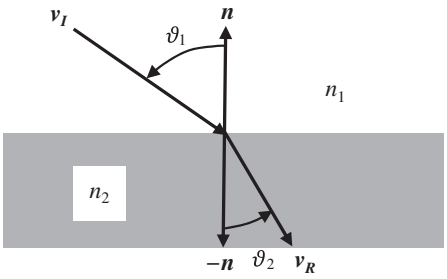

Figure 1.11 Illustration of the Snell–Descartes law of refraction.

1.6 Meshing and Indexing

The MCRT method used throughout this book requires that the modeling space be subdivided into surface and volume elements, i.e., that it be appropriately **meshed**. While entire books have been written on this topic alone, the limited treatment offered here is adequate for the needs of most MCRT analyses. The meshes used in the MCRT method must be amenable to **indexing**. Indexing refers to the process of systematically numbering the surface and volume elements in such a way that the numbers, called **indices**, can be determined algorithmically from the coordinates of a point lying on a surface element or within a volume element.

Pedagogical considerations favor limitation of the discussion presented here to rectilinear spaces, i.e., to spaces that can be represented by rectangular solid blocks. As used here, the word "solid" implies only that the spaces are three-dimensional. Many, if not most, enclosures of practical engineering interest can be accurately represented using a rectilinear mesh if care is taken to ensure that the surface element unit normal vectors represent the actual local curvature. The methods presented in this section can be extended to spaces consisting of trapezoidal, cylindrical (both circular and noncircular), and spheroidal solids.

Consider the hollow, three-dimensional rectilinear space illustrated in Figure 1.12. Use of the MCRT method often requires that the space be divided into N surface elements and $n - N$ volume elements, with a unique number, or "index", algorithmically assigned to each element. Furthermore, square surface elements and cubic volume elements are highly desirable. Finally, the resulting mesh must be sufficiently dense to assure adequate spatial resolution of the results obtained using an MCRT analysis. How do we go about satisfying all of these requirements? Consider the following numerical examples.

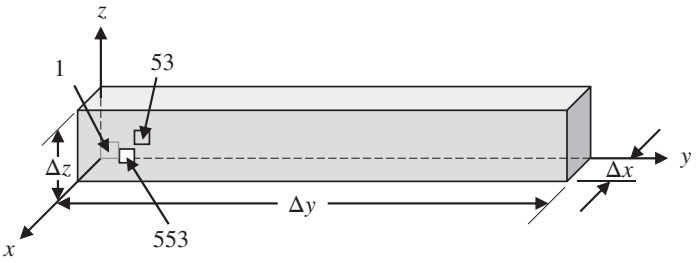

Figure 1.12 A hollow, three-dimensional rectilinear space.

Example 1.1

Suppose in Figure 1.12 that $\Delta x = 5.00$, $\Delta y = 50.00$, and $\Delta z = 10.00$, where the length units are arbitrary. The corresponding meshing solution, referred to as the **natural** solution, has five divisions in the x-direction ($n_x = 5$), 50 divisions in the y-direction ($n_y = 50$), and 10 divisions in the z-direction ($n_z = 10$). This meshing produces $2(n_x n_y + n_x n_z + n_y n_z) = N = 1600$ perfectly square surface elements and $n_x n_y n_z = n - N = 2500$ perfectly cubic volume elements. If it is found that the natural solution is too coarse to provide adequate spatial resolution in an eventual MCRT analysis, we simply multiply the number of divisions in each direction by the same integer to produce an acceptably dense mesh. On the other hand, if the mesh density is greater than needed – and therefore inefficient— we can always reduce it by dividing the number of divisions in each direction by n_x, n_y, or n_z, depending on which of the three values is smallest. This produces the minimal mesh that preserves the desirable property of square surface elements aligned with cubic volume elements. Such minimal meshes are referred to as **primitives**.

The general requirements for indexing are:

(i) element indices should be assigned algorithmically based on the coordinates of one of the element corners and, once assigned,
(ii) they should be algorithmically recoverable from the coordinates of any point on or within the element. The algorithm used for meshing is usually identical to the one used for indexing, but is used differently.

How do we index the space illustrated in Figure 1.12? All of the volume elements have six bounding surfaces, any one of which may be either real (i.e., a surface element) or imaginary (i.e., an interface between two adjoining volume elements). We have for any point (x, y, z) lying

within a given volume element; $x_{\min} \le x \le x_{\max}$, $y_{\min} \le y \le y_{\max}$, and $z_{\min} \le z \le z_{\max}$. We adopt the convention that the index number of a surface element lying in the y, z-plane at $x = 0$ is

$$i = y_{\max} + n_y\, z_{\min}, (x = 0); \tag{1.36}$$

while the index number of a surface element lying in the y,z-plane at $x = \Delta x$ is

$$i = y_{\max} + n_y\, z_{\min} + n_y n_z, (x = \Delta x). \tag{1.37}$$

All of the surface elements are assumed to face the interior of the rectangular solid. Note that the corner values of x, y, and z are all integers, thus assuring that the indices themselves are integers. Then, in the current example ($n_y = 50$ and $n_z = 10$),

$$\begin{aligned} i &= 1 \text{ when } y_{\max} = 1.00, z_{\min} = 0.00, \text{and } x = 0.00; \\ i &= 53 \text{ when } y_{\max} = 3.00, z_{\min} = 1.00, \text{and } x = 0.00; \\ \text{and} \quad i &= 553 \text{ when } y_{\max} = 3.00, z_{\min} = 1.00, \text{and } x = 5.00. \end{aligned}$$

Surface elements 1, 53, and 553 are indicated in Figure 1.12. It is left to the reader to puzzle out the expressions for the remaining surface element index numbers (Problem 1.20).

The corresponding expression for indexing the volume elements is

$$\begin{aligned} i &= N + x_{\max} + n_x\,(y_{\max} - 1) + n_x\, n_y\,(z_{\max} - 1) \\ &= 1600 + x_{\max} + 5\,(y_{\max} - 1) + 250\,(z_{\max} - 1). \end{aligned} \tag{1.38}$$

Derivation and validation of this result are left as an exercise (Problem 1.21). The process is further exemplified in Step 7, Section 5.3.

The MCRT method also requires that, given the x,y,z-coordinates somewhere on the walls of an enclosure, we be able to algorithmically recover the index number of the corresponding surface element. The logic that accomplishes this in the current example for surfaces in the y,z-plane at $x = 0$ is (see Problem 1.22):

$$\begin{aligned} &\text{for } x = 0; \text{if } y \ne 0 \text{ then } i = 1 + \mathit{floor}(y) + n_y\, \mathit{floor}(z), \\ &\qquad \text{else if } y = 0 \text{ then } i = 1 + n_y\, \mathit{floor}(z), \end{aligned} \tag{1.39}$$

where the *floor* operator in Matlab returns an integer equal to the real value of the argument truncated at the decimal point. For example, *floor*(5.57) = 5 and *floor*(0.57) = 0. Derivation and validation of the

expressions for indexing the remaining five walls and for indexing the volume element containing the point (x, y, z) are left as exercises (Problem 1.23).

Example 1.2

While the foregoing is an excellent "textbook" example, it is not very realistic. It is unlikely that the natural meshing solution will be exact. A more general and far more realistic case might be $\Delta x = 5.50$, $\Delta y = 51.25$, and $\Delta z = 9.75$. Note that, as in the foregoing example, the dimensions are given to one-hundredth of a unit. We begin by scaling the dimensions with respect to the smallest dimension, $\Delta x = 5.50$ in this case. Thus $\Delta x' = \Delta x/\Delta x = 1.00$, $\Delta y' = \Delta y/\Delta x = 51.25/5.50 = 9.32$, and $\Delta z' = \Delta z/\Delta x = 9.75/5.50 = 1.77$, where each result has been rounded to the nearest one-hundredth of a unit. Then the "natural" meshing in this case is $n_x = 100$, $n_y = 932$, and $n_z = 177$. As in the previous example, this meshing produces square surface elements and cubic volume elements. Furthermore, the elements are one unit on a side to within the precision of the given dimensions. Note that the natural meshing turns out to be the same as the primitive meshing in this example. However, if n_z had turned out to be 178 rather than 177, the primitive mesh would have been $n_x = 50$, $n_y = 466$, and $n_z = 89$. Finally, indexing proceeds in this general case just as in the special case considered in Example 1.1, since $x_{\min}$, $y_{\min}$, $z_{\min}$, $x_{\max}$, $y_{\max}$, and $z_{\max}$ are all integers.

We are now mathematically prepared to formulate and solve realistic radiation heat transfer and optics problems using the MCRT method. However, before moving directly into the main thrust of the book, we need to first establish fundamental knowledge of thermal radiation.

Problems

1.1 A plane whose unit normal vector $\boldsymbol{n} = \boldsymbol{k}$ intersects a sphere of radius R whose center is at (0, 0, 0). The radius of the disk formed by this intersection is $R/2$.

(a) In terms of R, what is the z-coordinate of the center of the disk?

(b) Determine if a ray emitted from $P_0 = (-R/2, 0, 0)$ in direction $(L, M, N) = (\sqrt{2}/2, 0, \sqrt{2}/2)$ intersects the disk. If so, where?

(c) In terms of R, where does the ray intersect the "cap" of the sphere lying above the disk?

1.2 A prolate spheroid (see Table 1.1) has a minor semi-axis of a, a major semi-axis of c (with $c > a$), and its center at $(0, y_C, 0)$. An x,z-plane intersects the spheroid at $0 < y_1 < a$, and a second x,z-plane intersects the spheroid at $y_1 < y_2 < a$. The intersections between the planes and the spheroid are ellipses with respective minor semi-axes of x_1 and x_2, and major semi-axes of z_1 and z_2. The values of x_1, y_1, z_1, x_2, y_2, and z_2 are considered to be known, and the values of a, b, and y_C are considered unknown. Derive explicit expressions for each of the three unknown quantities. Hint: You may want to make use of the Matlab symbolic solver feature.

1.3 Use the Matlab symbolic solver feature to solve Eq. (1.13) for t in terms of x_0, y_0, z_0, L, M, N, and R. Isolate and identify the coefficients A, B, and C in the solution.

1.4 Repeat Problem 1.3 for the case of a tri-axial ellipsoid whose center is located at (x_C, y_C, z_C). Use the symbols given in Table 1.1.

1.5 Repeat Problem 1.3 for the case of a two-sheet hyperboloid whose center is located at (x_C, y_C, z_C). The distance between the two vertices is $2c$. Use the symbols given in Table 1.1.

1.6 Repeat Problem 1.3 for the case of a right-circular cone whose center is located at (x_V, y_V, z_V). Use the symbols given in Table 1.1.

1.7 Repeat Problem 1.3 for the case of a right-circular cylinder whose center is located at (x_C, y_C, z_C). Use the symbols given in Table 1.1.

1.8 Demonstrate that if the quadratic coefficient $C = 0$ in Eq. (1.18), the line segment from point (x_0, y_0, z_0) to point (x_1, y_1, z_1) is a chord of the sphere.

1.9 The equation of a right-circular cone whose axis is parallel to the z-axis is given in Table 1.1. Consider the special case where $(x_v, y_v) = (0, 0)$, $z_v = 10$, and $\alpha = \pi/4$. A ray is emitted from $(x_0, y_0, z_0) = (-4, 2.5, 0)$ with direction cosines $(L, M, N) = (\sqrt{0.19}, 0, 0.9)$.

(a) Derive the equations for the quadratic coefficients A, B, and C.
(b) Solve the resulting quadratic equation for t_1 and t_2.
(c) Does the ray intersect the cone? If so, determine the coordinates of the candidate point or points of intersection.
(d) If two real points of intersection are found and only the inside surface of the cone is optically active, what are the direction

cosines of the reflected ray if the inside surface is an ideal mirror?

(e) If two real points of intersection are found and only the outside surface of the cone is optically active, what are the direction cosines of the reflected ray if the outside surface is an ideal mirror?

(f) For Parts (d) and (e), sketch the relevant cone surfaces and the incident and reflected rays.

1.10 Use Eqs. (1.20) and (1.22) to derive Eq. (1.23).

1.11 Verify that in order for a ray emitted from point (x_0, y_0, z_0) in direction (L, M, N) to intercept the wall of the spherical shell at point (x, y, z) it must be true that $\boldsymbol{v} \cdot \boldsymbol{n} < 0$.

1.12 Derive the three expressions in Eq. (1.34).

1.13 A hemispherical interior surface of radius 10 units is entirely located in the upper half-space ($z \geq 0$) with its center located at the origin of coordinates, (0, 0, 0), as shown in Figure 1.13. Write a computer program using Matlab (or equivalent) that traces 10 000 diffusely distributed rays from the origin into the hemisphere.

(a) Plot the points of intersection on the hemispherical surface.

(b) Show that the hemispherical surface can be subdivided into 10 equal-area bands by slicing it with nine parallel x,y-cutting planes at $z = 1, 2, 3, \ldots, 9$ units.

(c) Count the number of ray intersections in each band and then create a bar graph of these numbers as a function of the angle ϑ of the center of each band.

1.14 A condensing lens can be formed from the intersection of two spherical sectors of optical glass, as illustrated in Figure 1.14.

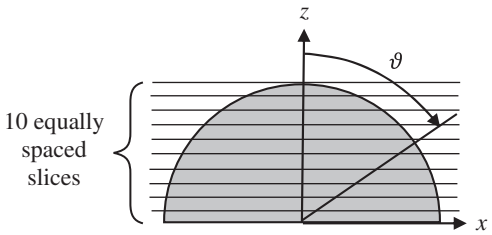

Figure 1.13 Geometry for Problem 1.13.

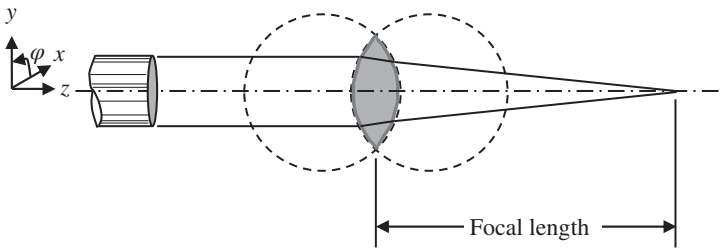

Figure 1.14 A condensing lens formed from two intersecting spherical sectors of optical glass.

The refractive index of air is 1.002772 and the refractive index of the optical glass used to construct the lens is 1.51681. The radius of curvature of both spherical sectors is 76.6 mm and the lens thickness at its center is 4.10 mm. A 5.0-mm diameter collimated beam is incident to the lens. A spatially uniform beam may be well simulated by emitting 1000 rays parallel to the optical axis of the lens at random x,y-locations in the source plane. If the center of the circular source of diameter D is located at $(x, y, z) = (0, 0, 0)$, the radial distance from the center is

$$r = (D/2)\ \sqrt{R_r}, \tag{1.40}$$

where R_r is a random number uniformly distributed between 0 and 1. A random angle φ, measured with respect to the x-axis, may be defined by a second random number, R_φ,

$$\varphi = 2\pi R_\varphi. \tag{1.41}$$

Then the x,y-coordinates of a random emission site are

$$x = r\ \cos\varphi, y = r\ \sin\varphi, \text{and } z = 0. \tag{1.42}$$

(a) Plot the randomly distributed emission in the plane of the source.
(b) Plot the paths of the rays from the source through the lens to their focal point. [Hint: You will need the vector form of the Snell-Descartes law,

$$\begin{aligned} \boldsymbol{v_R} &= (n_1/n_2)\,\boldsymbol{n} \times (-\boldsymbol{n} \times \boldsymbol{v_I}) \\ &\quad - \boldsymbol{n}\,[1 - (n_1/n_2)^2\,(\boldsymbol{n} \times \boldsymbol{v_I}) \cdot (\boldsymbol{n} \times \boldsymbol{v_I})]^{1/2}, \end{aligned} \tag{1.43}$$

where $\boldsymbol{n}$ is the local surface unit normal vector, $\boldsymbol{v_I}$ is the incident vector, and $\boldsymbol{v_R}$ is the refracted vector.]

(c) What is the focal length of this lens?

1.15 Derive the vector form of the Snell–Descartes law, Eq. (1.43).

1.16 The equation of a certain right-circular cone is

$$S(x, y, z) = x^2 + y^2 - (z - z_v)^2 \tan^2\alpha = 0, \tag{1.44}$$

where z_v is the z-location of its vertex and α is its half-angle.

(a) Use the Microsoft Word "draw" feature (Insert→Shapes) to sketch the full cone, showing both branches, or "sheets." Label the x-, y-, and z-axes and the angle α.

(b) Derive the expression for the inward-directed unit normal vector $\boldsymbol{n}$ for the upper sheet. By convention, the inward-directed unit normal vector for the upper sheet has a positive z-component.

(c) Derive the expression for the unit tangent vector $\boldsymbol{t_1}$ for the upper sheet that lies entirely in the surface and points toward the vertex.

(d) Derive the expression for the second unit tangent vector $\boldsymbol{t_2}$ that is mutually orthogonal to both the unit normal vector and the first unit tangent vector. Assure that the three vectors define a right-hand system.

(e) Add the three unit vectors to your sketch.

1.17 The equation of a right circular cylindrical surface is

$$S(x, y) = x^2 + y^2 - R^2 = 0, \tag{1.45}$$

where R is the radius.

(a) Use the Microsoft Word "draw" feature (Insert→Shapes) to sketch a right circular surface between $-L \le z \le L$. Label the x-, y-, and z-axes and the radius R.

(b) Derive the expression for the inward-directed unit normal vector $\boldsymbol{n}$.

(c) Derive the expression for the unit tangent vector $\boldsymbol{t_1}$ that lies entirely in the surface and points in the positive-z direction.

(d) Derive the expression for the second unit tangent vector $\boldsymbol{t_2}$ that is mutually orthogonal to both the unit normal vector and the first unit tangent vector. Assure that the three vectors define a right-hand system.

(e) Add the three unit vectors to your sketch.

1.18 The equation for an elliptic paraboloid is

$$S(x, y, z) = x^2 + y^2 - a(z - z_v) = 0, \tag{1.46}$$

where $a(z - z_v)$ is the radius of its "rim" at a distance z from its vertex at z_v.

(a) Use the Microsoft Word "draw" feature (Insert→Shapes) to sketch an elliptic paraboloid. Label the x-, y-, and z-axes.
(b) Derive the expression for the inward-directed unit normal vector $\boldsymbol{n}$.
(c) Derive the expression for the unit tangent vector $\boldsymbol{t_1}$ that lies entirely in the x,y-plane and points in the counter-clockwise direction looking down on the x,y-plane.
(d) Derive the expression for the second unit tangent vector $\boldsymbol{t_2}$ that is mutually orthogonal to both the unit normal vector and the first unit tangent vector. Assure that the three vectors define a right-hand system.
(e) Add the three unit vectors to your sketch.

1.19 Consider the wedge-shaped cavity depicted in Figure 1.15.

(a) Show that the equation for the sloped surface is

$$S(y, x) = z - (y_{\max} - y)/\tan\alpha = 0. \tag{1.47}$$

(b) Derive the expression for the inward-directed unit normal vector $\boldsymbol{n}$ on the sloped surface.
(c) Derive the expression for the first unit tangent vector $\boldsymbol{t_1}$ on the sloped surface.
(d) Suppose $\alpha = 40°$ and that, during a Monte Carlo ray-trace, angles of $\vartheta = 34.6°$ and $\varphi = 102.4°$ are obtained for the reflection of a given ray from the sloped surface. What are the direction cosines L, M, N of the path of the reflected energy bundle?
(e) Suppose the point of reflection corresponding to Part (d) lies at the center of the sloped surface and that $y_{\max} = 180.5\,\mu\text{m}$. Which surface does the reflected energy bundle strike and what are the coordinates of the point of intersection of the ray with the surface? Show the ray on a reasonably scaled drawing.

1.20 Consider the hollow, three-dimensional rectilinear space of Figure 1.12. Derive the expressions for the remaining surface element index numbers i following Eqs. (1.36) and (1.37).

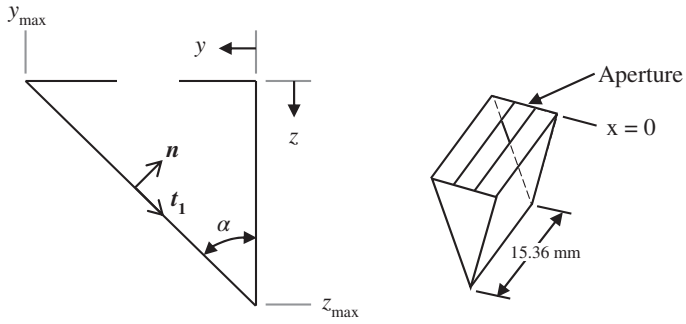

Figure 1.15 The wedge-shaped cavity of Problem 1.19.

1.21 Derive Eq. (1.38).

1.22 Derive Eq. (1.39).

1.23 Derive and validate the expressions for indexing the remaining five walls, as mentioned below Eq. (1.39).

1.24 Derive the expression for computing the index of the volume element containing the point (x, y, z) following Eq. (1.37).

1.25 Figure 1.16 shows a hollow box whose walls have been subdivided into four square surface elements. Compose and test an algorithm-based Matlab (or equivalent) function to index the surface elements of the box based on knowledge of the appropriate corner coordinates when $\Delta x = \Delta y = \Delta z = 2.00$. Use the MS Word drawing tool to sketch and fully label the box for both the natural and the primitive meshing schemes.

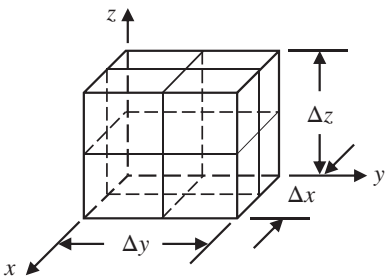

Figure 1.16 Geometry for Problems 1.25 and 1.26.

1.26 For the hollow box shown in Figure 1.16, compose an algorithm-based Matlab (or equivalent) function for finding the surface element number based on the x,y,z-coordinates of a wall point. (The algorithm composed for meshing in Problem 1.25 should work here as well.) Test the algorithm using $(x, y, z) = (1.45, 0.27, 2{,}00)$.

Reference

1. Mahan, J.R. (2002). *Radiation Heat Transfer: A Statistical Approach*. New York: Wiley.